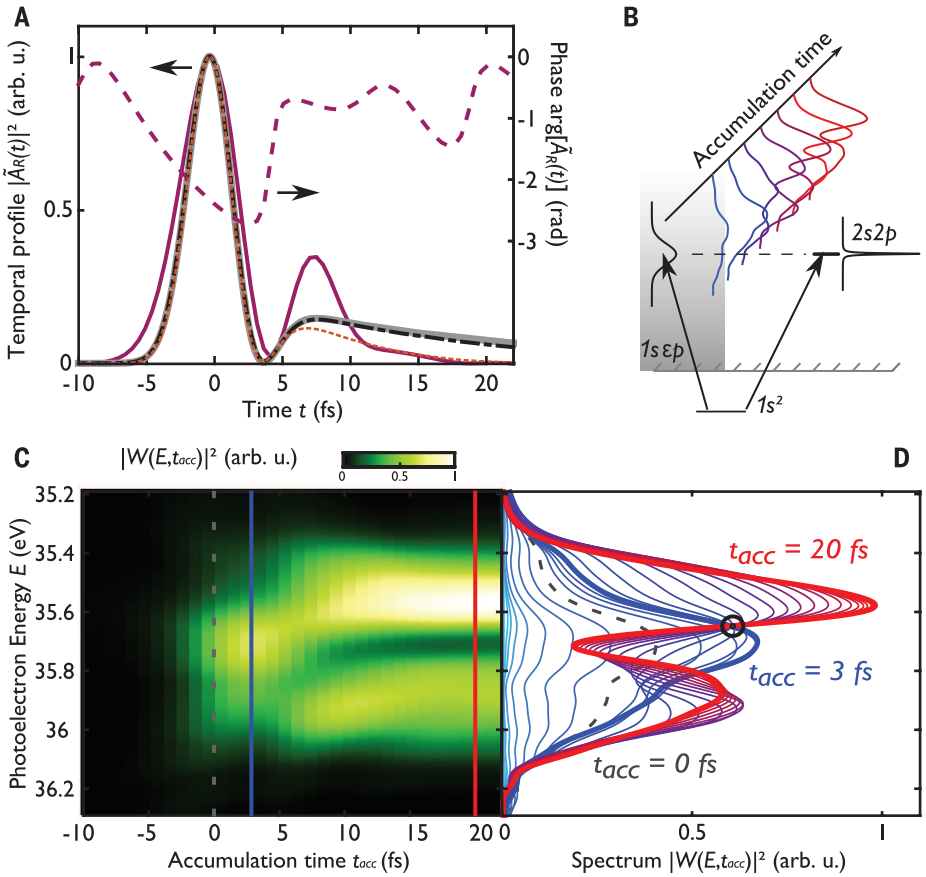

Fig. 3. Resonant EWP in the time domain and time-resolved reconstruction of the resonance buildup. (**A**) Temporal profile of the resonant EWP obtained by Fourier transform of the SB_{64} data (i) from the experimental spectrogram (solid purple curve) and corresponding temporal phase (dashed purple curve), and (ii) from the simulated spectrogram, taking into account (dotted orange curve), or not (dot-dashed black curve), the finite spectrometer resolution. The latter fully coincides with the one-photon resonant EWP profile from a direct analytical calculation (solid gray curve) (*25*), thereby demonstrating the validity of our interferometric technique. (**B**) Illustration of the formation dynamics of the resonant spectrum resulting from interference between the two paths in the Fano autoionization model. (**C**) Reconstruction of the time-resolved buildup of the resonant spectrum using the time-energy analysis introduced in Eq. 5. The photoelectron spectrum is plotted as a function of the upper temporal limit (accumulation time t_{acc}) used for the inverse Fourier transform. The dashed gray curve, solid blue curve, and solid red curve indicate accumulation times of 0, 3, and 20 fs, respectively. (**D**) Lineouts of (C) every 1 fs. This figure evidences first the growth of the direct path until a maximum is reached at ~3 fs (blue curves), and then the increasing spectral interference with the resonant path that finally results in the Fano line shape (red curves). At 35.6 eV, an isosbestic-like point is crossed by all curves from 3 fs onward (black circle), evidencing a position in the final line shape where only the direct path contributes.

(*24*). The temporal profile $\tilde{A}_R(t)$ thus decomposes into a Gaussian nonresonant term and a resonant contribution, like our experimental data (Fig. 3A). The destructive temporal interference between the two terms leads to the amplitude minimum and phase jump identified around t = 4 fs.

To illustrate how the interference between the two paths governs the formation of the resonance line shape, Wickenhauser *et al.* (*17*) introduced a time-frequency analysis based on the limited inverse Fourier transform:

$$W(E,t_{acc}) = \int_{-\infty}^{t_{acc}} \tilde{A}_R(t) \exp\left(\frac{iEt}{\hbar}\right) dt \qquad (5)$$

which shows how the spectrum builds up until accumulation time t_{acc}. The result of this transform applied to the experimental EWP in Fig. 3A is shown in Fig. 3, C and D. The chronology of the resonance formation can be nicely interpreted within Fano's formalism. In a first stage until ~3 fs, a close-to-Gaussian spectrum reflecting the ionizing harmonic spectral shape emerges: The direct path to the continuum dominates. Then the resonant path starts contributing as the populated doubly excited state decays in the continuum: Interferences coherently build up until ~20 fs, consistent with the temporal profile in Fig. 3A, to eventually converge toward the asymmetric measured spectrum. The resonance growth can thus be decomposed in two nearly consecutive steps governed by fairly different time scales.

The buildup of the resonant profile reveals the presence of a notable point around E = 35.6 eV where, as soon as the direct ionization is completed, the spectrum barely changes with t_{acc} any longer. This can be explained by splitting the $|R(E)|^2$ spectrum from Eq. 3 into three terms:

$$|R(E)|^2 = 1 + \frac{q^2+1}{\varepsilon^2+1} + 2\frac{q\varepsilon - 1}{\varepsilon^2+1} \qquad (6)$$

(*26*). At this isosbestic-like point—that is, for $\varepsilon = [(1/q) - q]/2$—the bound (second term) and coupling (third term) contributions ultimately cancel each other, leaving only the direct continuum contribution (first term). This point thus gives a useful landmark in the resonant line shape (e.g., for cross section calibration or reference purposes).

Spectrally resolved electron interferometry thus provides insight into the ultrafast strongly correlated multielectron dynamics underlying autoionization decay. Given the generality and wide applicability of the Fano formalism [see, e.g., (*26*)], we anticipate that our approach, combined with progress in attosecond pulse production and particle detection (e.g., access to photoelectron angular distributions), will open prospects for studies of complex photoemission dynamics close to resonances and, more generally, structured EWP dynamics in a variety of systems, from molecules (*27*–*29*) and nanostructures (*26*) to surfaces (*10*). Furthermore, the well-defined amplitude and phase distortions induced by the resonance offer a means for shaping the broadband EWP, bringing opportunities for coherent control in the attosecond regime.

REFERENCES AND NOTES

1. F. Krausz, M. Ivanov, *Rev. Mod. Phys.* **81**, 163–234 (2009).
2. M. Hentschel *et al.*, *Nature* **414**, 509–513 (2001).
3. P. M. Paul *et al.*, *Science* **292**, 1689–1692 (2001).
4. Y. Mairesse, F. Quéré, *Phys. Rev. A* **71**, 011401(R) (2005).
5. M. Chini, S. Gilbertson, S. D. Khan, Z. Chang, *Opt. Express* **18**, 13006–13016 (2010).
6. M. Schultze *et al.*, *Science* **328**, 1658–1662 (2010).
7. K. Klünder *et al.*, *Phys. Rev. Lett.* **106**, 143002 (2011).
8. R. Pazourek, S. Nagele, J. Burgdörfer, *Rev. Mod. Phys.* **87**, 765–802 (2015).
9. S. Haessler *et al.*, *Phys. Rev. A* **80**, 011404 (2009).
10. A. L. Cavalieri *et al.*, *Nature* **449**, 1029–1032 (2007).
11. S. B. Schoun *et al.*, *Phys. Rev. Lett.* **112**, 153001 (2014).
12. M. Sabbar *et al.*, *Phys. Rev. Lett.* **115**, 133001 (2015).
13. M. Kotur *et al.*, *Nat. Commun.* **7**, 10566 (2016).
14. U. Fano, *Phys. Rev.* **124**, 1866–1878 (1961).
15. S. Gilbertson *et al.*, *Phys. Rev. Lett.* **105**, 263003 (2010).
16. M. Domke, K. Schulz, G. Remmers, G. Kaindl, D. Wintgen, *Phys. Rev. A* **53**, 1424–1438 (1996).
17. M. Wickenhauser, J. Burgdörfer, F. Krausz, M. Drescher, *Phys. Rev. Lett.* **94**, 023002 (2005).
18. Z.-H. Loh, C. H. Greene, S. R. Leone, *Chem. Phys.* **350**, 7–13 (2008).
19. C. Ott *et al.*, *Science* **340**, 716–720 (2013).
20. C. Ott *et al.*, *Nature* **516**, 374–378 (2014).